ISSN 0021-3640, JETP Letters, 2024, Vol. 120, No. 12, pp. 932–938. © The Author(s), 2024. This article is an open access publication.
Russian Text © The Author(s), 2024, published in Pis'ma v Zhurnal Eksperimental'noi i Teoreticheskoi Fiziki, 2024, Vol. 120, No. 12, pp. 970–976.

MISCELLANEOUS

Numerical Simulation of a Photonic Tensor Core for the Hardware Acceleration of the Optical Matrix–Vector Multiplication

G. A. Kolosov[a], A. S. Shorokhov[a], and A. A. Fedyanin[a,*]

[a] *Faculty of Physics, Moscow State University, Moscow, 119991 Russia*

**e-mail: fedyanin@nanolab.phys.msu.ru*

Received October 11, 2024; revised November 5, 2024; accepted November 12, 2024

A realistic numerical model of a photonic tensor core based on the crossbar architecture with absorbing GeSbTe chalcogenide glass films as weight elements of a photonic matrix has been developed. The performance of the model for the matrix–vector multiplication has been demonstrated. The possibility of using the tensor core based on the implemented architecture in convolutional neural networks for image recognition tasks has been shown. Numerical simulations have been used for the first time to estimate the potential performance and energy efficiency of a photonic hardware accelerator, taking into account the modern experimental element base.

DOI: 10.1134/S0021364024603956

1. INTRODUCTION

Technological difficulties in the fabrication of nanostructures, as well as quantum effects, e.g., tunneling electrons through a very small gate, fundamentally limit the size of transistors. The traditional layout of von Neumann computers involves separate placement of the processor and memory, which leads to the so-called von Neumann bottleneck limiting the performance [1]. The importance of machine learning and artificial intelligence tasks, the results of which are used in a large number of applications: speech and image recognition, medical diagnostics, prediction of material properties, etc. [2–4], increases the demand for hardware computing accelerators in neural networks. Most of the calculations include matrix–vector multiplication; therefore, it is of the most relevant importance to accelerate this operation.

In image processing tasks, the use of fully connected neural networks is inappropriate due to the excessive number of free parameters; as a result, overtraining occurs; i.e., the algorithm adjusts to the training sample and does not work well on target data. To solve this problem, a convolutional neural network approach was developed [5, 6], in which an input image is preprocessed by a system of digital filters before entering the input of the decisive fully connected neural network.

In recent years, many electronic digital and analog accelerators have been developed [7, 8], but they also exhibit problems of high power consumption due to heat generation and limitation of computing speed due to the need to recharge parasitic capacities.

Photonic accelerators [9], including those in the form of a photonic tensor core (PTC), i.e., an integral accelerator [10], are aimed at parallel processing of data directly in memory. The advantages of this approach include low computational latency and high parallelism of computations when using multiplexing of different wavelengths into a single channel of the input vector.

Phase-changing materials, in particular, chalcogenide glasses, such as GeSbTe [11, 12], Sb_2Se_3 [13], etc., provide a promising physical platform for the implementation of the weight elements of the PTC matrix. Such materials can rapidly change their phase state from amorphous to crystalline and vice versa under optical or electrical heating. Different phase states of a phase-changing material have different refractive indices, which makes it possible to accurately control optical radiation in phase-changing material nanostructures.

The key advantage of phase-changing structures is the energy independence of the phase state: the energy is consumed only when switching the weight specified by the structure, which is especially important for calculations in the convolutional neural network, the specificity of which is to multiply many different input vectors by the same weight matrix during image processing with a digital filter.

To prove the competitiveness of the PTC approach, it is necessary to know the energy efficiency and performance of the PTC. In previous studies, these characteristics were evaluated analytically [14], which could lead to overestimated values. The purpose

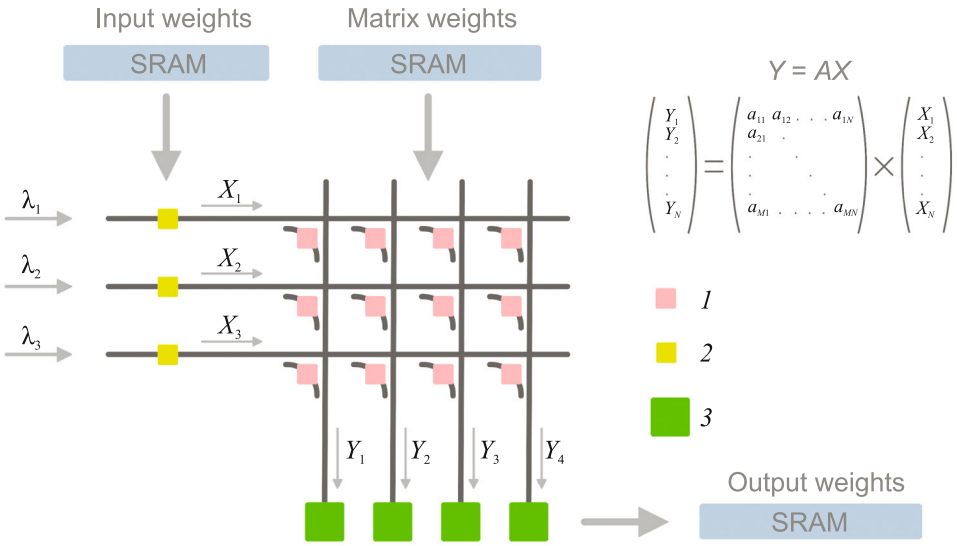

Fig. 1. (Color online) Diagram of the architecture of an incoherent crossbar array: (*1*) ideal modulator or GST absorber, (*2*) microring or Mach–Zehnder modulator, and (*3*) PIN diode with the amplifier and low-pass filter. The input and matrix weights are loaded from the static random access memory (SRAM). The output vector, after being read by the detector array, is loaded back into the SRAM.

of this work is to obtain the key characteristics of the PTC from a numerical simulation.

2. METHODS

In this work, using the method of transient processes in *S* matrices, we constructed a model of the PTC with the crossbar architecture (see Fig. 1) [11]. Such an architecture can be implemented in two fundamentally different ways: incoherent and coherent. In the incoherent architecture, each channel of the input vector corresponds to an individual radiation wavelength for the possibility of demultiplexing the output signal along wavelengths. In contrast, the PTC in the coherent architecture, operates at a single wavelength, which leads to the difficult problem of phase tuning of the system to ensure constructive interference [15]. We chose the incoherent implementation of the PTC, which, in particular, allows the use of methods for additional compression of the processed information flow [16, 17], which is schematically presented in Fig. 2.

Microring and Mach–Zehnder modulators were considered for the channel-by-channel modulation of input vector radiation. The advantages of the former modulators include their small geometric dimensions (down to 10 μm in diameter [18]) and high modulation frequencies [19], while the disadvantages include a high *Q*-factor of resonance [20], which requires the thermal adjustment of the fabricated modulator [18]. Mach–Zehnder modulators, in turn, have significantly larger geometric dimensions [21], which will negatively affect the possible scaling of the system. For the above reasons, we chose microring modulators because the weight representation with an accuracy of 9 bit was experimentally demonstrated [22].

For the correct detection of the output signal in an incoherent circuit, it is necessary to smooth out radiation beatings at the detector, which are due to the pres-

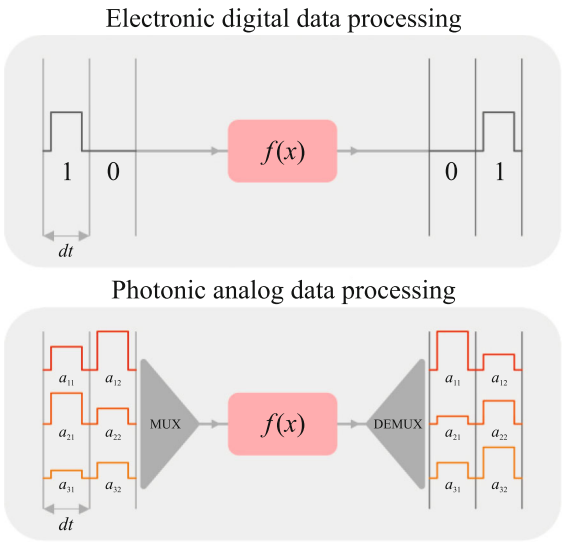

Fig. 2. (Color online) Data processing in the (upper panel) electronic accelerator and (lower panel) photonic tensor core. In the photonic tensor core, the input weight is presented in the analog form opposed to the digital representation in the electronic accelerator. The photonic tensor core also allows the additional compression of the information flow by multiplexing different wavelengths into one channel, i.e., allows one to simultaneously multiply several input vectors by the weight matrix.

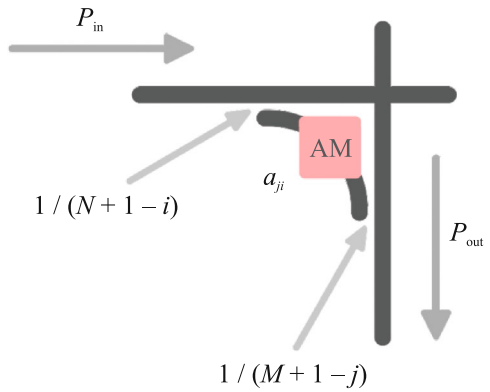

Fig. 3. (Color online) Schematic representation of the weight element of the photonic tensor core. The arrows indicate the direction of radiation propagation and the coupling coefficients of the directional coupler.

ence of close wavelengths in one channel of the output vector. For this purpose, a low-pass filter and a transimpedance amplifier with the operating parameters selected by minimizing the bit error rate in the matrix–vector multiplication were placed at the detector output,.

GeSbTe (GST) films with a thickness of 10 nm placed on the top of a silicon waveguide were chosen as the weight elements of the matrix, where the amorphous state ($n = 3.98 + 0.042i$ [23]) with a high transmittance and the crystalline state with a low transmittance ($n = 6.49 + 1.054i$ [23]) were taken as unity and zero, respectively. The attenuation of the waveguide mode in the structure was calculated by the finite difference method. The accuracy of the matrix weight was taken to be less than or equal to 6 bit [11], which is the maximum obtained so far in the experiment for integral GST nanostructures.

The calculations also involved realistic losses in all elements of the circuit and the dispersion of directional couplers, since the dispersion of the other elements of the circuit is significantly less (except for microring modulators, but their dispersion is compensated by thermal tuning). The dispersion of directional couplers was calculated by the expression [24]

$$P_{cross} = \kappa P_{in} = \sin^2\left(\frac{\pi\delta n}{\lambda}\right) P_{in}. \quad (1)$$

Here P_{in} is the radiation power at the input of the coupler, P_{cross} the power in the parallel waveguide after the coupler has passed, κ is the coupling coefficient of the directional coupler, and δn is the difference in the effective refractive indices of the symmetric and antisymmetric modes in the coupled section of the directional coupler, which was also calculated by the finite difference method. Coupling coefficients κ in directional couplers depend on the position of a particular element in the photonic matrix, which is reflected in Fig. 3. The final relation between the input and output radiation powers in the element is specified in the form

$$P_{out} = P_{in} \frac{a_{ij}}{(N - i + 1)(M - j + 1)}, \quad (2)$$

where a_{ij} is the weight of the element in the ith row and jth column in the matrix specified by the GST film and N and M are the numbers of rows and columns, respectively. Such coupling coefficients are necessary for each element of the matrix to receive the same radiation power [11].

Artificial noise and displacements of no more than half of the bit interval were introduced into the input and matrix weights of the system during the simulation in order to ensure nearly real simulation conditions and to estimate the number of bit errors at the output of the system, i.e., its stability and accuracy. All operating parameters of the model are summarized in Table 1.

Table 1. Parameters of the photonic tensor core

Parameter	Value
Modulation frequency	≤10 GHz
Central laser frequency	193.1 THz
Frequency interval	≥0.1 THz [14]
Low-pass filter cutoff frequency	18 GHz
Amplifier resistance	2 kΩ
Input weights	≤9 bit [22]
Matrix weights	≤6 bit [11]

3. RESULTS

Using the constructed model, the multiplication of a random input vector by a random matrix with weights in the range from 0 to 1 was demonstrated using the PTC with dimensions from 2 × 2 to 9 × 9 (see supplementary material for more details). Using a quantizer (with an accuracy of 6 bit), we obtained a signal picture in the digital domain at the output of the amplifier, which made it possible to calculate the bit error rate of the analog matrix–vector multiplication compared to the reference matrix–vector multiplication produced by the NumPy library. A bit error was considered to be the fall of the output weight of the analog matrix–vector multiplication and the output weight of the control matrix–vector multiplication into different quantization levels. The minimization of the bit error rate was used to further optimize the electronic strapping of the detector.

The multiplication by the photonic core shows a high accuracy within the confidence interval of the output vector with the maximum possible accuracy of

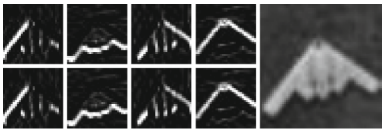

Fig. 4. (Upper images) Reference convolution using the NumPy library and (lower images) the convolution with the photonic tensor core. The right image is the original image from the CIFAR-10 dataset.

6 bit, which is limited from above by the bit accuracy of setting the matrix weights. The numerical simulation results show that an increase in the accuracy of setting input weights and matrix weights above 5 bit hardly affects the bit error rate, since the dispersion of the directional couplers begins to have a significant effect.

In order to study the applicability of the PTC to deep learning problems, we examined the efficiency of transferring the base layers of the neural network to the optical analog domain. To this end, the efficiency of the convolution operation using the PTC was compared to the reference obtained using the NumPy library. For this purpose, the convolution of various images from the CIFAR-10 dataset was carried out using four horizontal and vertical 3 × 3 filters, which were transferred into a 9 × 4 photonic matrix. The input vector was obtained by converting from a two-dimensional matrix corresponding to a region of the image into a one-dimensional array of values with subsequent normalization. Since negative weights cannot be implemented in the selected architecture, the convolution result was postprocessed in the case of the PTC matrix with the NumPy library using the expression

$$B_{\text{real}} = 2B_{\text{core}} - IA_{\text{in}}, \quad (3)$$

where B_{real} is the required output vector, B_{core} is the result of multiplication in the PTC, I is the identity matrix, and A_{in} is the input vector. In the future, it is possible to implement negative weights using either a mode-converting metasurface [25] or balanced detection approaches from the architecture of a microring weight bank [26]. The results of numerical simulation of the convolution are presented in Fig. 4.

After demonstrating the performance of the model in the problems of forward pass of the convolutional neural network, we studied the scaling potential of the crossbar array. To estimate the maximum size of the PTC at the specified parameters of the model, the output power of the system was calculated at the maximum (i.e., unit) input and matrix weights– the optical budget. The power of the minimum useful signal at the output of the PTC (at the maximum input weights and a diagonal matrix with the minimum nonzero weights) was also compared to the power of optical noise in the system (at the maximum input weights and zero matrix weights). More information about the matrices used and the method to obtain the maximum array size is given in the supplementary material. The results of the calculations are presented in Fig. 5. The dependence of the desired signal on the size of the crossbar matrix is non-monotonic because of destructive beats due to the presence of many wavelengths in the output channel.

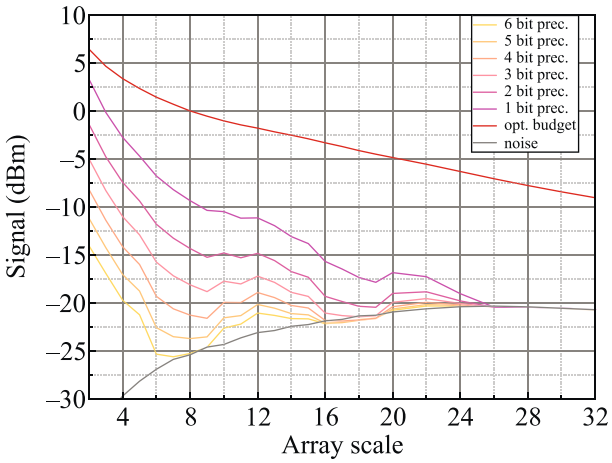

Fig. 5. (Color online) Numerically estimated minimum desired signal versus the linear size of the square matrix array. The minimum useful signal significantly depends on the accuracy of setting the weights in the array.

The 1:1 ratio of the minimum signal to noise, i.e., a difference in power of 3 dBm was chosen as a criterion of achieving the maximum size of the PTC, because this ratio will make it possible to distinguish between two minimum nonzero signal levels. The final data for the maximum possible size of the PTC are shown in Fig. 6. The decrease in the array size with an

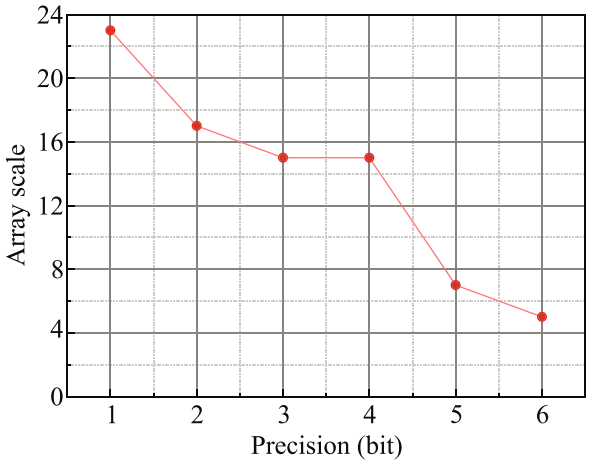

Fig. 6. (Color online) Numerically estimated maximum linear size of the array versus the accuracy of setting the matrix weights.

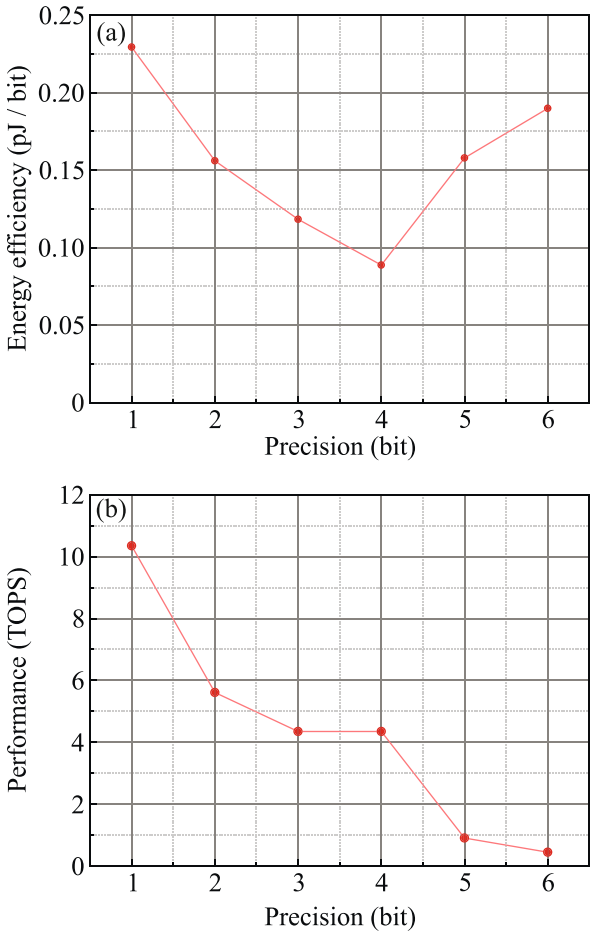

Fig. 7. (Color online) (a) Numerically estimated energy efficiency of the system versus the required computational accuracy. (b) Numerically estimated system performance versus the required computational accuracy.

increase in the accuracy of calculations is non-monotonic due to destructive beats in the calculations of the minimum useful signal. The estimation was carried out depending on the accuracy of setting the matrix weights, correspondingly, on the maximum accuracy of the final calculations. The key parameters in this simulation are losses on each element in the system summarized in Table 2.

Table 2. Losses on elements of the photonic tensor core

Element	Value, dBm
Laser (input power)	10 [27]
Waveguide	–180 per meter
Directional coupler	–0.1 [28]
Waveguide intersection	–0.03 [29]
Noise in the intersection of waveguides	–37 [29]
Microring modulator	–0.1 [30]
GST absorber	–0.5 [31]

To understand the applicability of the PTC, it is necessary to evaluate its energy efficiency and performance in units of tera operations per second (TOPS). These parameters increase with the size of the PTC. Accordingly, it is necessary to use simulation data to determine the maximum size of the PTC. Using modern experimental data on the energy consumption of the active elements of the photonic matrix from Table 3, we estimated the energy efficiency of the system depending on the bit size of the matrix weights and, correspondingly, the maximum accuracy of calculations. To ensure a constant flow of input data and load of weight data, a neural network model needs a developed memory hierarchy with a global buffer in the form of DRAM, through which information is exchanged with the electronic computing part, as well as a local SRAM for quick access to the input and matrix weights. A more detailed analysis of the memory hierarchy and its parameters can be found in [32, 33]. The power consumption of memory access [34] was also taken into account in the model.

In the calculations, it was assumed that the matrix elements are switched once every 1000 multiplication cycles, which approximately corresponds to the problem of convolution of a 32 × 32 pixel image. When estimating the performance of the PTC, the multiplication and addition operations performed during the matrix–vector multiplication were taken as a single operation. Estimates of the energy efficiency and performance are presented in Fig. 7. It is seen that the performance of the PTC increases with a decrease in the accuracy of calculations and the core power consumption has a minimum at a computational accuracy of 4 bit.

4. CONCLUSIONS

To summarize, simulating the photonic tensor core on the crossbar architecture, we have shown that the most energetically optimal application of the 15 × 15 photonic tensor core is ensured with microring modulators of the input vector with a modulation rate of 10 GHz and the 4 bit accuracy of setting the matrix weights; in this case, the performance of the core will be about 4 TOPS with a power consumption of less

Table 3. Power consumption of elements of the photonic tensor core

Element	Power consumption
Laser	10 mW, efficiency up to 25% [35]
Microring modulator	500 fJ/bit with thermal adjustment 40 fJ/bit without thermal adjustment [18]
GST absorbers	20 pJ/switch [23]
Detector and amplifier	2.3 pJ/bit [36]
Access to the memory	3.9 pJ/bit [34]

than 0.1 pJ/bit. The performance of one photonic tensor core is comparable to electronic accelerators; i.e., many cores in a photonic accelerator will significantly increase not only the energy efficiency, but also the performance.

The performance and energy efficiency of the photonic tensor core can be further increased by its multiparametric optimization using reverse engineering methods [37, 38], as well as by the use of several wavelength packages in parallel. It is also necessary to optimize directional couplers, waveguide intersections, modulators, and other elements of the system. The use of metasurfaces for mode conversion will reduce radiation losses in the weight elements, which will also have a positive effect on the maximum size of the matrix.

SUPPLEMENTARY INFORMATION

The online version contains supplementary material available at https://doi.org/10.1134/S0021364024603956.

FUNDING

This work was supported by the Russian National Center for Physics and Mathematics (direction no. 1 "National Center for Research of Supercomputer Architectures. Stage 2023–2025") and by the Not-for-Profit Foundation for the Development of Science and Education "Intellect."

CONFLICT OF INTEREST

The authors of this work declare that they have no conflicts of interest.

OPEN ACCESS

REFERENCES

1. W. Aspray, *John von Neumann and the Origins of Modern Computing* (MIT Press, Cambridge, 1990).
2. F. Amato, A. López, E. M. Pena-Méndez, P. Vaňhara, A. Hampl, and J. Havel, J. Appl. Biomed. **11**, 47 (2013).
3. Q. Li, W. Cai, X. Wang, Y. Zhou, D. D. Feng, and M. Chen, IEEE **13**, 844 (2014).
4. A. A. Popkova and A. A. Fedyanin, JETP Lett. **118**, 502 (2023).
5. J. Gu, Z. Wang, J. Kuen, L. Ma, A. Shahroudy, B. Shuai, T. Liu, X. Wang, G. Wang, J. Cai, and T. Chen, Pattern Recogn. **77**, 354 (2018).
6. H. J. Yoo, IEIE SPC **4**, 35 (2015).
7. C. Zhang, P. Li, G. Sun, Y. Guan, B. Xiao, and J. Cong, in *Proceedings of the 2015 ACM/SIGDA International Symposium on Field-Programmable Gate Arrays* (Assoc. Comput. Machinery, New York, 2015), p. 161.
8. K. Ovtcahrov, O. Ruwase, J. Y. Kim, J. Fowers, K. Strauss, and E. S. Chung, Microsoft Res. Whitepaper **2**, 1 (2015).
9. A. I. Musorin, A. S. Shorokhov, A. A. Chezhegov, T. G. Baluyan, K. R. Safronov, A. V. Chetvertukhin, A. A. Grunin, and A. A. Fedyanin, Phys. Usp. **66**, 1211 (2023).
10. M. Miscuglio and V. J. Sorger, Appl. Phys. Rev. **7**, 31404 (2020).
11. F. Brückerhoff-Plückelmann, J. Feldmann, C. D. Wright, H. Bhaskaran, and W. Pernice, J. Appl. Phys. **129**, 151103 (2021).
12. J. Zheng, A. Khanolkar, P. Xu, S. Colburn, S. Deshmukh, J. Myers, J. Frantz, E. Pop, J. Hendricksin, J. Doylend, N. Boechler, and A. Majumdar, Opt. Mater. Express **8**, 1551 (2018).
13. M. Delaney, I. Zeimpekis, D. Lawson, D. Hewak, and O. Muskens, Adv. Funct. Mater. **30**, 2002447 (2020).
14. J. Feldmann, N. Youngblood, M. Karpov, H. Gehring, X. Li, M. Stappers, M. Le Gallo, X. Fu, A. Lukashchuk, A. S. Raja, J. Liu, C. D. Wright, A. Sebastian, T. J. Kippenberg, W. H. P. Pernice, and H. Bhaskaran, Nature (London, U.K.) **589**, 7840 (2021).
15. N. Youngblood, IEEE J. Sel. Top. Quantum Electron. **29**, 1 (2022).
16. B. Dong, S. Aggarwal, W. Zhou, U. E. Ali, N. Farmakidis, J. S. Lee, Y. He, X. Li, D. L. Kwong, C. D. Wright, W. Pernice, and H. Bhaskaran, Nat. Photon. **17**, 1080 (2023).
17. F. Brückerhoff-Plückelmann, J. Feldmann, H. Gehring, W. Zhou, C. D. Wright, H. Bhaskaran, and W. Pernice, Nanophotonics **11**, 4063 (2022).
18. P. Dong, R. Shafiiha, S. Liao, H. Liang, N. N. Feng, D. Feng, G. Li, X. Zheng, A. V. Krishnamoorthy, and M. Asghari, Opt. Express **18**, 10941 (2010).
19. Y. Zhang, H. Zhang, J. Zhang, J. Liu, L. Wang, D. Chen, N. Chi, X. Xiao, and S. Yu, Photon. Res. **10**, 1127 (2022).
20. W. Bogaerts, P. De Heyn, T. van Vaerenbergh, K. De Vos, S. K. Selvaraja, T. Claes, P. Dumon, P. Bienstmanm, D. van Thourhout, and R. Baets, Laser Photon. Rev. **6**, 47 (2012).
21. M. R. Watts, W. A. Zortman, D. C. Trotter, R. W. Young, and A. L. Lentine, IEEE J. Sel. Top. Quantum Electron. **16**, 159 (2010).
22. W. Zhang, C. Huang, H. T. Peng, S. Bilodeau, A. Jha, E. Blow, T. F. de Lima, B. J. Shastri, and P. Prucnal, Optica **9**, 579 (2022).

23. D. Wu, X. Yang, N. Wang, L. Lu, J. Chen, L. Zhou, and B. Rahman, Nanophotonics **11**, 3437 (2022).
24. A. Yariv, IEEE J. Quantum Electron. **9**, 919 (1973).
25. C. Wu, H. Yu, S. Le, R. Peng, I. Takeuchi, and M. Li, Nat. Commun. **12**, 96 (2021).
26. A. N. Tait, M. A. Nahmias, B. J. Shastri, and P. R. Prucha, J. Light. Technol. **32**, 4029 (2014).
27. S. Keyvaninia, G. Roelkens, D. van Thourhout, C. Jany, M. Lamponi, A. Le Lieprve, F. Lelarge, D. Make, G. H. Duan, D. Bordel, and J. M. Fedeli, Opt. Express **21**, 3784 (2013).
28. M. A. Al-Qadasi, L. Chrostowski, B. J. Shastri, and S. Shekhar, APL Photon. **7**, 20902 (2022).
29. S. Wu, X. Mu, L. Cheng, S. Mao, and H. Y. Fu, Micromachines **11**, 326 (2020).
30. S. Manipatruni, K. Preston, L. Chen, and M. Lipson, Opt. Express **18**, 18235 (2010).
31. Z. Yu, J. Zheng, P. Xu, W. Zhang, and Y. Wu, IEEE Photon. Technol. Lett. **30**, 250 (2017).
32. C. Demirkiran, F. Eris, G. Wang, J. Elmhurst, N. Moore, N. C. Harris, A. Basumallik, V. J. Reddi, A. Joshi, and D. Bunadar, J. Emerg. Technol. Comput. Syst. **19**, 1 (2023).
33. D. Sturm and S. Mozaeni, in *Proceedings of the 2023 Design, Automation and Test in Europe Conference and Exhibition DATE* (EDA Consortium, San Jose, 2023), p. 1.
34. M. O'Connor, N. Chatterjee, D. Lee, J. Wilson, A. Agrawal, S. W. Keckler, and W. J. Dally, in *Proceedings of the 50th Annual IEEE/ACM International Symposium on Microarchitecture* (Assoc. Comput. Machinery, New York, 2017), p. 41.
35. B. R. Koch, E. J. Norberg, J. E. Roth, B. Kim, A. Ramaswamy, R. S. Guzzon, J. Hutchinson, J. H. Shin, J. Imamura, B. Gomez, G. Fish, and A. Fang, in *Proceedings of the Novel In-Plane Semiconductor Lasers XIII,* Proc. SPIE **9002**, 72 (2014).
36. S. Nayak, A. H. Ahmed, A. Sharkia, A. S. Ramani, S. Mirabbassi, and S. Shekhar, IEEE Trans. Circuits Syst. I: Regul. Pap. **66**, 3162 (2019).
37. K. R. Safronov, V. O. Bessonov, and A. A. Fedyanin, JETP Lett. **114**, 321 (2021).
38. M. Wei, X. Lin, K. Xu, Y. Wu, C. Wang, Z. Wang, K. Lei, K. Bao, J. Li, L. Li, E. Li, and H. Lin, Nanophotonics **13**, 2183 (2024).

Translated by R. Tyapaev